Machine learning-based programmed cell death-related index to predict prognosis and immunotherapy response in skin cutaneous melanoma

XINYI WANG[1*], YUZHI ZHENG[2*], SHAN YANG[1], HONGLI SI[1], WENQIU CHEN[1] and SIYUAN SHEN[3]

[1]Department of Dermatology, Shenzhen Yantian District People's Hospital, Shenzhen, Guangdong 518000, P.R. China;
[2]Department of Dermatology, Dapeng New District Nan'ao People's Hospital, Shenzhen, Guangdong 518000, P.R. China;
[3]Department of Dermatology, Affiliated Cixi Hospital, Wenzhou Medical University, Ningbo, Zhejiang 315300, P.R. China

Received July 3, 2025; Accepted August 18, 2025

DOI: 10.3892/ol.2025.15327

Abstract. Skin cutaneous melanoma (SKCM) is a highly aggressive malignancy with heterogeneous outcomes and a variable response to immunotherapy. Programmed cell death (PCD) serves a key role in tumor progression and immune regulation, but its prognostic and therapeutic relevance in SKCM remains to be elucidated. An integrative machine learning strategy encompassing 77 algorithm combinations was employed to construct a PCD-related index (PCDI). Associations between the PCDI and immune microenvironment, immunotherapy response and drug sensitivity were also investigated. Subsequently, a 13-gene risk signature was identified via the Lasso algorithm and used to calculate a PCDI-based risk score. Functional enrichment and experimental validation were conducted to explore potential biological functions of stratifin (SFN), which had the highest positive coefficient in the formula used to calculate the PCDI-based risk score. The PCDI robustly stratified patients into high- and low-risk groups with markedly different overall survival across The Cancer Genome Atlas and Gene Expression Omnibus cohorts. The risk score outperformed traditional clinical parameters in predicting prognosis and served as an independent prognostic factor. Low-risk patients exhibited higher immune cell infiltration, immune checkpoint expression and tumor immunogenicity, as well as lower tumor immune dysfunction and exclusion, and immune escape scores. The model predicted improved immunotherapy responses in low-risk groups, which was further validated in three independent immunotherapy cohorts. By contrast, high-risk patients were more sensitive to chemotherapeutic and targeted agents. Using the Cell Counting Kit-8 assay, SFN, one of the key genes in the signature, was experimentally validated as an oncogenic driver in SKCM. The present study developed and validated a machine learning-based PCDI that effectively predicts prognosis and immunotherapy response in SKCM. This PCDI provides novel insights into PCD-mediated tumor-immune interactions and demonstrates potential for personalized therapeutic decision-making in melanoma.

Correspondence to: Professor Xinyi Wang, Department of Dermatology, Shenzhen Yantian District People's Hospital, 2010 Wutong Road, Shatoujiao, Yantian, Shenzhen, Guangdong 518000, P.R. China
E-mail: wangxyi3@yeah.net

*Contributed equally

Key words: programmed cell death, machine learning, skin cutaneous melanoma, immune response

Introduction

Skin cutaneous melanoma (SKCM) is a highly aggressive malignancy originating from melanocytes, with increasing global incidence and poor prognosis despite recent advances in immunotherapy and targeted therapy (1). In 2020, >320,000 new cases of SKCM were diagnosed worldwide, with nearly 57,000 related deaths (2). SKCM is primarily associated with exposure to ultraviolet radiation, whether from natural sunlight or indoor tanning practices (3). The management of SKCM involves various therapeutic approaches, such as surgery, radiotherapy, targeted therapy and immunotherapy, with the choice of treatment determined according to the disease stage (4). Although immune checkpoint inhibitors (ICIs) have revolutionized treatment paradigms in advanced SKCM, notable inter-patient heterogeneity leads to variable therapeutic responses, underscoring the need for novel biomarkers to guide personalized therapy.

Programmed cell death (PCD) is a fundamental biological process involved in tumor progression, immune evasion and therapeutic resistance (5). Various PCD modes, including apoptosis, pyroptosis, ferroptosis, necroptosis, autophagy and the newly defined cuproptosis, have been shown to influence cancer immunity and treatment outcomes (6). Increasing evidence indicates that PCD-related genes (PRGs) serve multifaceted roles in modulating the tumor microenvironment (TME) and shaping antitumor immunity (7). For example, high expression of ferroptosis regulators has been associated with immune cell infiltration and response to ICIs in

several cancer types (8,9). In lung adenocarcinoma, a machine learning-derived PCD signature was shown to associate with prognosis, immune infiltration levels and immunotherapy sensitivity (10,11). A PCD signature could also serve as a prognostic biomarker for ovarian cancer (12), bladder cancer (13) and hepatocellular carcinoma (14). However, the clinical relevance and prognostic value of PCD-related gene expression in SKCM, particularly in the context of immunotherapy, have not been fully elucidated.

With the advancement of high-throughput sequencing and computational methods, machine learning has emerged as a powerful tool for integrating multi-dimensional genomic data to uncover clinically relevant biomarkers. Compared with traditional statistical approaches, machine learning algorithms such as Lasso, CoxBoost, survivalSVM and random survival forest offer greater flexibility and accuracy in modeling complex gene-phenotype relationships and building predictive models with high generalizability (15,16).

In the present study, a novel PCD-related index (PCDI) was developed for SKCM using integrative machine learning strategies. The predictive efficacy of the PCDI was systematically evaluated in terms of prognosis and response to immunotherapy, providing a potential tool for precision oncology in patients with SKCM.

Materials and methods

Data acquisition and pre-processing. Transcriptomic and clinical data of patients with SKCM were downloaded from The Cancer Genome Atlas (TCGA; TCGA-SKCM dataset; n=425) database on November 10, 2023. Three independent validation cohorts were retrieved from the Gene Expression Omnibus (GEO, https://www.ncbi.nlm.nih.gov/geo/) database, namely, GSE54467 (n=79) (17), GSE59455 (n=122) (18) and GSE65904 (n=210) (19). Three immunotherapy datasets [GSE91061 (20), GSE78220 (21) and IMvigor210 (22)] were used to assess the predictive value of PCDI in treatment response.

A total of 15 types of PCD patterns (for example, apoptosis, necroptosis, ferroptosis, pyroptosis and autophagy) were included and PCD-related genes were curated from Molecular Signatures Database (https://www.gsea-msigdb.org/gsea/msigdb/index.jsp), Kyoto Encyclopedia of Genes and Genomes (https://www.kegg.jp/), GeneCards (https://www.genecards.org/) and a recent study (13) (Table SI). Differential expression analysis (|log fold change| ≥1.5 and adjusted P<0.05) between tumor and normal samples was conducted using the 'limma' R package (version 3.64.3) (23) and prognostic genes were screened using univariate Cox regression analysis (P<0.05).

Construction of the PCDI. The present study employed an integrative machine learning pipeline comprising 10 algorithms (Lasso, Ridge, CoxBoost, random survival forest, survival-support vector machines, efficient neural network, partial least squares regression for Cox, super partial correlation, stepwise Cox and gradient boosting machine) to develop and evaluate 77 model combinations. The present study developed the PCDI in four steps following the methods of a previous study (24): i) Univariate Cox regression was used to investigate prognostic biomarkers (TCGA); ii) a total of 77 algorithm combinations were then fitted to the prediction model (TCGA); iii) all algorithm combinations were carried out in GEO cohorts; and iv) the concordance (C)-index was computed for each cohort. Detailed parameters of the 10 machine learning algorithms are described in Data S1. The model with the highest average C-index across TCGA and GEO cohorts was selected as the optimal PCDI. Patients were stratified into high- and low-PCDI (risk score) groups (cut-off value: 0.135) using the 'surv_cutpoint' function of the 'survminer' R package. Kaplan-Meier survival analysis with log-rank test and time-dependent receiver operating characteristic (ROC) curves were used to assess the prognostic capability of PCDI. The clinical outcome of patients with SKCM was analyzed through both univariate and multivariate Cox regression models to identify potential risk factors associated with the disease. Based on PCDI score and additional clinical features (age, sex, TNM stage, T stage, N stage and M stage), the 'nomogramEx' program (https://cran.r-project.org/web/packages/nomogramEx/index.html) was used to construct a predicting nomogram.

Evaluation of immunotherapeutic value. Immune infiltration was evaluated using the 'immunedeconv' R package (version 1.0) (25), integrating CIBERSORT, TIMER and other tools. Tumor microenvironment components (immune, stromal and ESTIMATE scores) were assessed via the 'estimate' package (version 4.4.0) (26). To predict immunotherapy response, the present study analyzed the tumor mutation burden (TMB) (27), tumor immune dysfunction and exclusion (TIDE) score (28), and immunophenoscore (29), as well as immune escape score calculated with an immune escape gene set (CD47, ADAM10, HLA-G, CD274, FASLG, CCL5, TGFB1, IL10, PTGER4) from a previous study (30). TMB is an emerging biomarker of sensitivity to ICIs and has been shown to be associated with response to programmed cell death protein 1 (PD-1) and programmed death-ligand 1 (PD-L1) blockade immunotherapy (26). TIDE is a computational tool used to evaluate tumor immune escape mechanisms and predict the response to ICI treatment. The immunophenoscore is a notable predictor of response to anti-cytotoxic T-lymphocyte associated protein 4 (CTLA-4) and anti-PD-1 therapy. The immune escape score is an indicator used to evaluate the ability of tumor cells to evade immune system surveillance and killing. The predictive value of PCDI was further validated in three independent immunotherapy cohorts (GSE91061, GSE78220 and IMvigor210). Gene set enrichment analysis (GSEA) and single sample GSEA (ssGSEA) were conducted to explore pathway differences between high and low PCDI groups. Subsequently, the 'oncoPredict' R package (version 1.2) (31) was employed to estimate the IC_{50} values of therapeutic agents for SKCM cases, utilizing data from the Genomics of Drug Sensitivity in Cancer database (https://www.cancerrxgene.org/).

Human Protein Atlas (HPA) database. The HPA database (http://www.proteinatlas.org) utilizes transcriptomic and proteomic technologies to explore protein expression at the RNA and protein levels in different human tissue types and organs. The HPA database is a convenient way to explore the expression levels of stratifin (SFN), which had the highest

positive coefficient in the formula for calculating PCDI score, in normal and tumor tissue. Representative immunohistochemical images of SFN staining in normal and SKCM tissues were obtained from the 'Tissue' and 'Cancer' sections of the HPA.

Cell culture. Melanoma cell lines (A375, A2058, MV3, Sk-mel-1 and Sk-mel-28) and a normal skin-derived cell line (PIG1) were obtained from The Cell Bank of Type Culture Collection of The Chinese Academy of Sciences. These cells were cultured in RPMI-1640 medium enriched with 10% FBS (Procell Life Science & Technology Co., Ltd.) and 1% antibiotic solution (Procell Life Science & Technology Co., Ltd.). Cells were maintained at 37˚C in an atmosphere containing 5% CO_2.

Cell transfection. To achieve SFN gene silencing, the melanoma A375 and A2058 cell lines were separately transfected with si-SFN (cat. no. siG000002810A-1-5; sequence 5'-GCA ATTAGTATTGTTTGAAACAT-3') or si-negative control (cat. no. siN0000001-4-10; sequence 5'-GCAGGATGG GATAAGTCTAAA-3') sequences provided by Guangzhou RiboBio Co., Ltd. A total of 0.5 nmol siRNA was used for transfection each time using Lipofectamine® 3000 (Thermo Fisher Scientific, Inc.). A375 and A2058 cells were transfected with siRNA at 37˚C for 48 h before further experiments were performed.

Reverse transcription-quantitative PCR (RT-qPCR). Total RNA was extracted from the aforementioned cells (A375, A2058, MV3, Sk-mel-1, Sk-mel-28 and PIG-1) using Triquick® Reagent (Beijing Solarbio Science & Technology Co., Ltd.). According to the manufacturer's protocol, complementary DNA (cDNA) for SFN was synthesized from the isolated RNA employing the SweScript RT I FTTSt Strand cDNA Synthesis Kit (cat. no. G3330-100; Wuhan Servicebio Technology Co., Ltd.). The resulting cDNA was then used as a template for qPCR analysis performed on a PCR system using 2X SYBR Green qPCR Master Mix (Low ROX) (cat. no. G3321-05; Selleck China). The thermocycling conditions were as follows: Initial denaturation at 95˚C for 5 min; followed by 35 cycles at 95˚C for 30 sec, 55˚C for 30 sec and 70˚C for 30 sec. Gene expression levels were quantified using the $2^{-\Delta\Delta Cq}$ method and normalized to GAPDH expression (32). Primer sequences used were as follows: GAPDH forward (F), 5'-GTCTCCTCT GACTTCAACAGCG-3' and GAPDH reverse (R), 5'-ACC ACCCTGTTGCTGTAGCCAA-3'; and SFN F, 5'-TCCACT ACGAGATCGCCAACAG-3' and SFN R, 5'-GTGTCAGGT TGTCTCGCAGCA-3'.

Cell Counting Kit-8 (CCK-8) assay. To evaluate cell viability, transduced A375 and A2058 cells were seeded into 96-well plates and allowed to grow for 24, 48 or 72 h. After incubation, CCK-8 reagent (cat. no. G1613-1ML Wuhan Servicebio Technology Co., Ltd.) was added to each well, followed by a 4-h incubation at 37˚C. Absorbance values were measured at 450 nm using a microplate reader.

Statistical analysis. All statistical analyses were conducted using R software (version 4.2.1; R Development Core Team). Differences between continuous variables were assessed using either the Wilcoxon rank-sum test or unpaired Student's t-test, depending on data distribution. Pearson's correlation coefficients were calculated to evaluate associations between two continuous parameters. Kaplan-Meier survival curves were compared using the two-sided log-rank test Univariate and multivariate Cox regression analyses were performed to identify risk factors for the overall survival of patients with SKCM. $P<0.05$ was considered to indicate a statistically significant difference. All assays were repeated three times.

Results

Identification of prognostic PRGs in SKCM. To explore the prognostic value of PRGs in SKCM, the present study first identified differentially expressed genes (DEGs) between tumor and normal tissues from the TCGA-SKCM cohort. A total of 1,638 genes were found to be significantly dysregulated ($|\log_2 FC|>1.5$; $P<0.05$) (Fig. S1A). By intersecting these DEGs with a curated set of 1,254 PRGs, the present study obtained 117 differentially expressed PRGs (Fig. S1B). Among them, univariate Cox regression identified 54 PRGs that were significantly associated with overall survival (OS) in patients with SKCM (Fig. S1C), suggesting their potential utility for constructing a prognostic model.

Integrative machine learning-based PCDI. Using the 54 prognosis-associated PRGs, the present study applied a machine learning integration strategy involving 77 algorithm combinations across TCGA and GEO datasets. Based on the average C-index across training and validation cohorts, the Lasso algorithm was identified as the optimal method, achieving the highest predictive performance (Fig. 1A). The optimal λ parameter was selected when the partial likelihood deviance reached its minimum in cross-validation and 13 PRGs were retained to construct the PCDI (Fig. 1B). The risk score for each patient was calculated as: Risk score=(0.029 x SFN^{exp}) + (-0.176 x IDS^{exp}) + (-0.054 x $SCFD1^{exp}$) + (-0.591 x $TRIM34^{exp}$) + (-0.011 x $CD74^{exp}$) + (-0.023 x $FBXW7^{exp}$) + (−0.045 x $CRIP1^{exp}$) + (-0.133 x $IFNAR2^{exp}$) + (-0.051 x $PIM2^{exp}$) + (-0.053 x $CTSW^{exp}$) + (-0.008 x $NUPR1^{exp}$) + (-0.029 x $ICAM1^{exp}$) + (-0.024 x $AIM2^{exp}$).

Patients in the TCGA, GSE65904, GSE54467 and GSE59455 cohorts were stratified into high- and low-risk groups based on the optimal cut-off (0.1365). Kaplan-Meier survival analyses demonstrated that patients in the high-risk group consistently exhibited worse OS compared with that of the low-risk group across all datasets (Fig. 1C-F). Time-dependent ROC analyses further confirmed the predictive robustness of the model, with 1-, 3- and 5-year AUCs >0.70 in the majority of cohorts. The AUC of the 1-, 3- and 5-year ROC curve was 0.888, 0.800 and 0.787 in the TCGA cohort (Fig. 1C), 0.749, 0.829 and 0.791 in the GSE65904 cohort (Fig. 1D), 0.643, 0.850 and 0.926 in the GSE54467 cohort (Fig. 1E), and 0.916, 0.770 and 0.720 in the GSE59455 cohort (Fig. 1F), respectively.

Evaluation of the performance of PCDI. To further assess the clinical utility of the risk signature, the present study compared its predictive accuracy against standard clinical

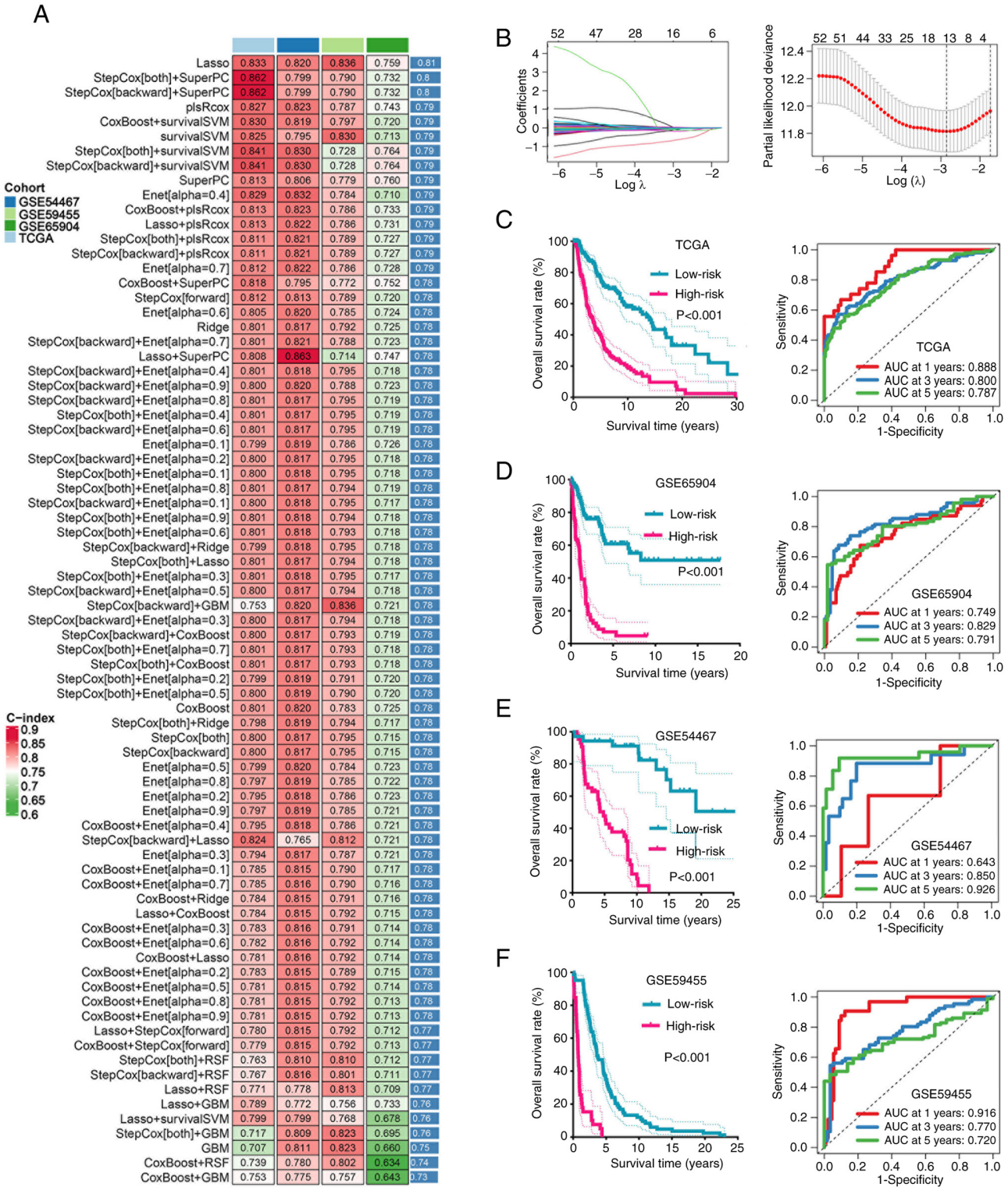

Figure 1. Machine learning developed programmed cell death-related signature. (A) The C-index of 77 types of prognostic models of TCGA and GEO cohorts. (B) Determination of the optimal λ was obtained when the partial likelihood deviance reached the minimum value in the TCGA cohort and further generated Lasso coefficients of the most useful prognostic genes. The survival curve and their corresponding ROC curve in SKCM with different risk score in (C) TCGA, (D) GSE65904, (E) GSE54467 and (F) GSE59455 dataset. C-index, concordance index; TCGA, The Cancer Genome Atlas; GEO, Gene Expression Omnibus; GSE, gene expression data series; SKCM, skin cutaneous melanoma; RSF, random survival forest; survivalSVM, survival-support vector machines; Enet, efficient neural network; plsRCox, partial least squares regression for Cox; SuperPC, super partial correlation; GBM, gradient boosting machine; AUC, area under the curve.

parameters. C-index analysis revealed that the risk score consistently outperformed age, sex and TNM stage in all cohorts (33) (Fig. 2A-D). Univariate and multivariate Cox regression analyses confirmed that the risk score was an independent predictor of OS in SKCM (Fig. 2E and F). A prognostic nomogram integrating the risk score and clinical

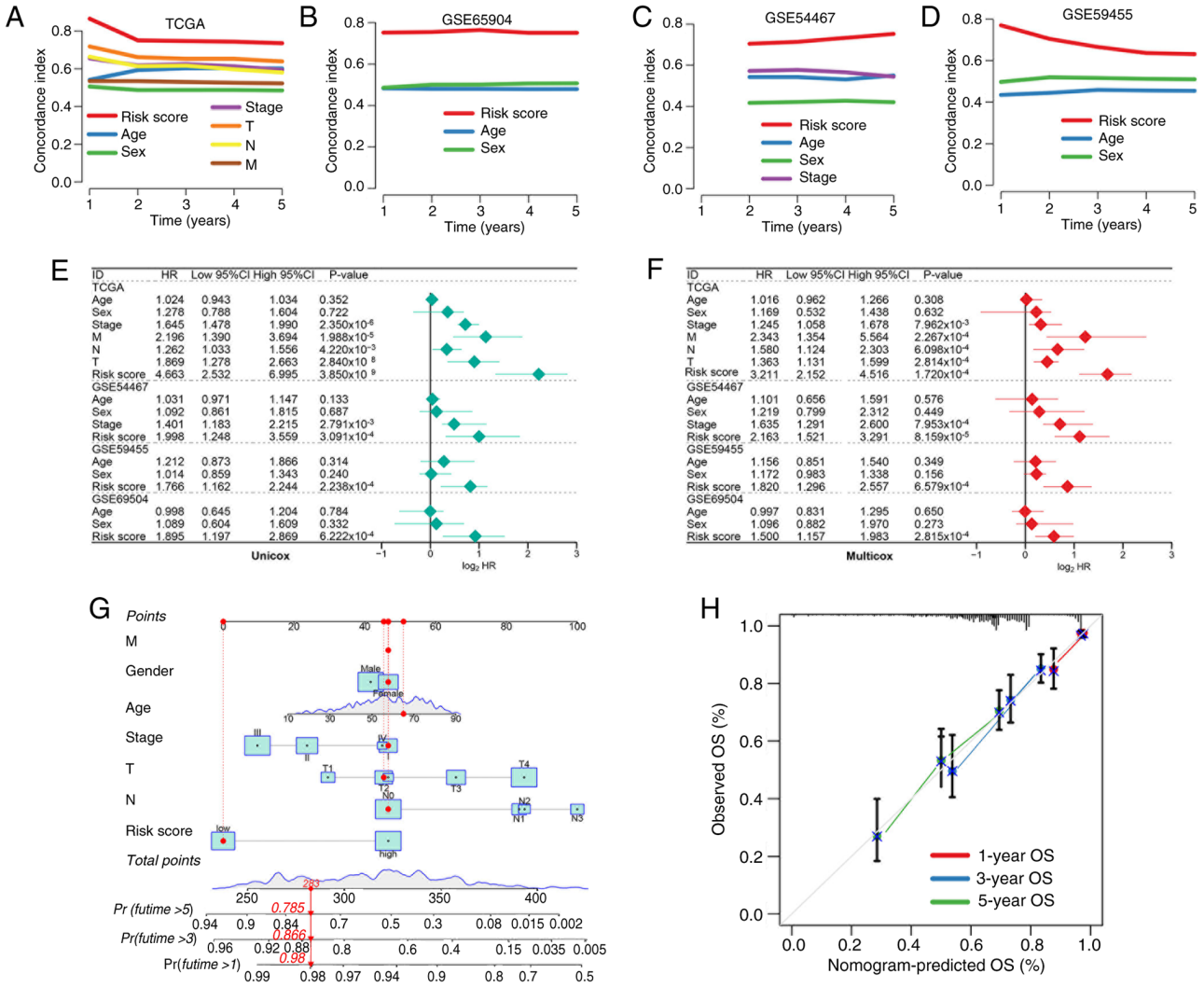

Figure 2. Performance of programmed cell death-related signature in predicting the prognosis in SKCM. C-index comparing the performance of programmed cell death-related signature and clinical characteristics in predicting the prognosis of SKCM in (A) TCGA, and (B) GSE65904, (C) GSE54467 and (D) GSE59455 cohorts. (E) Univariate and (F) multivariate Cox regression analysis identified the risk factors for the overall survival of patients with SKCM. (G) A nomogram constructed using programmed cell death-related signature and clinical characteristics. (H) Calibration plots suggested that the actual 1-, 3- and 5-year survival times were highly consistent with the predicted survival times. C-index, concordance index; TCGA, The Cancer Genome Atlas; SKCM, skin cutaneous melanoma; GSE, gene expression data series; HR, hazard ratio; OS, overall survival.

features (for example, pT and pN stage) was constructed (Fig. 2G) and calibration plots demonstrated notable agreement between predicted and observed survival probabilities (Fig. 2H).

Immune landscape in high- and low-risk groups. Due to the known association between PCD and immune modulation, the present study investigated the immune infiltration profiles of patients with SKCM with different risk scores. Multiple deconvolution algorithms revealed significant negative correlations between the risk score and immune cell abundance (Fig. 3A). Particularly, $CD8^+$ T cells, M1 macrophages and dendritic cells were significantly negatively correlated with risk score in SKCM (Fig. 3B-D). ssGSEA analysis further indicated lower immune cells and immune function scores, including aDCs, B cells, $CD8^+$ T cells, mast cells, NK cells, TILs, T helper (Th) cells, Th2 cells, APC_co_stimulation, cytolytic activity, inflammation promoting and T cell co-stimulation, human leukocyte antigen (HLA), parainflammation and type II IFN response in the high-risk group (Fig. 3E and F). Patients with low-risk score also exhibited significantly higher stromal, immune and ESTIMATE scores, which suggested a more active tumor immune microenvironment (Fig. 3G).

Association between risk score and immunotherapy response. To evaluate the predictive value of the risk signature in immunotherapy response, the present study examined multiple immune-related features. Patients with SKCM with low-risk score had significantly higher expression of HLA-related genes and immune checkpoint molecules compared with patients with SKCM and a high-risk score (Fig. 4A and B). Elevated expression levels of HLA-related genes predicted a higher chance of immunotherapy benefits (34). Furthermore, they demonstrated increased TMB score and PD-1/CTLA4 immunophenoscores, suggesting enhanced tumor immunogenicity (Fig. 4C and D). A marked response to immunotherapy is indicated by low TIDE and

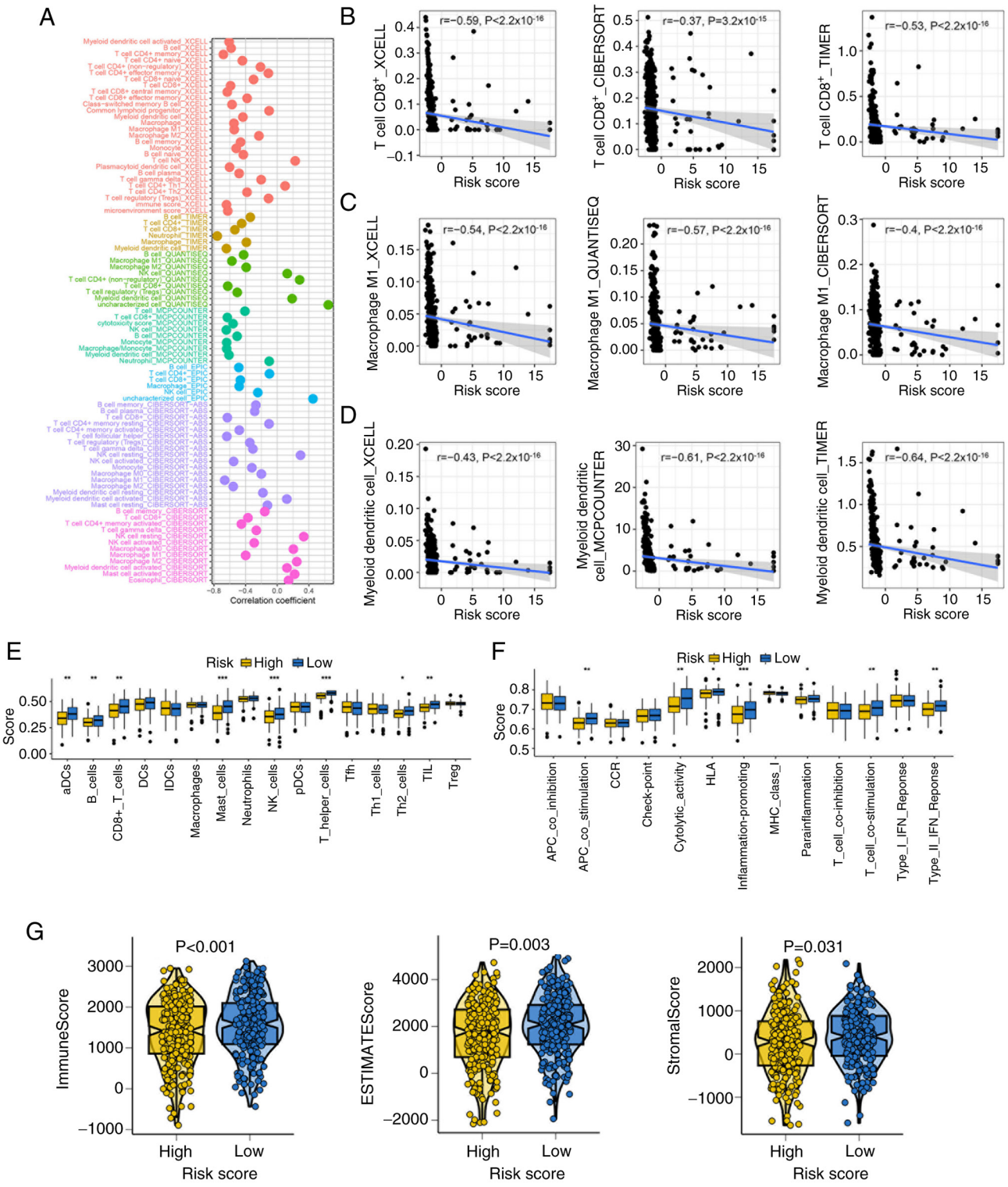

Figure 3. Landscape of the immune infiltration among various risk score groups. (A) Correlation between risk score and immune cell abundance, determined using seven algorithms. The correlation between the risk score and the number of (B) $CD8^+$ T cells, (C) M1 macrophages and (D) dendritic cells. ssGSEA study assessing (E) immune cell and (F) immune-related function levels across several risk score categories. (G) The stromal, immune and ESTIMATE scores across various risk score categories. *P<0.05, **P<0.01 and ***P<0.001. ssGSEA, single sample gene set enrichment analysis; aDCs, antibody-drug conjugates; DCs, dendritic cells; NK, natural killer; Tfh, T follicular helper cells; Th, T helper cells; TIL, tumor infiltrating lymphocytes; Treg, regulatory T cells; APC, antigen presenting cells; CCR, chemokine receptor; MHC, major histocompatibility complex; iDCs, immature dendritic cells; pDCs, plasmacytoid dendritic cells.

immune escape scores (28,35). In the present study, low-risk score patients with SKCM had lower TIDE, immune escape and immune surveillance scores, indicating a more favorable immunotherapy profile (Fig. 4E-G). These findings were further validated in three independent melanoma immunotherapy cohorts. In the IMvigor210, GSE78220 and GSE91061 datasets, the risk score of non-responders in SKCM was notably greater compared with that of responders, and low-risk patients exhibited higher response rates and improved survival outcomes compared with high-risk

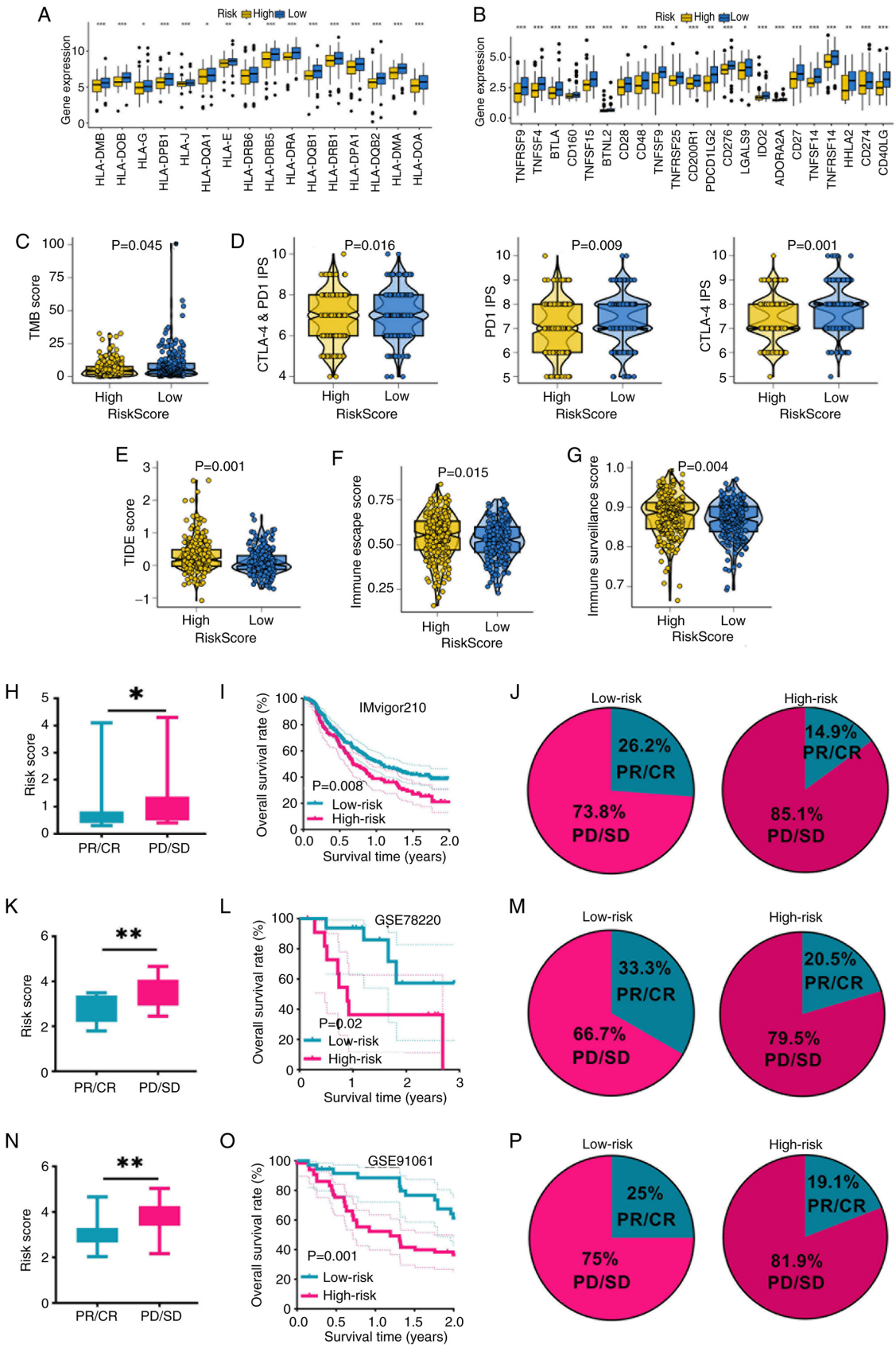

Figure 4. Programmed cell death-related signature acted as a biomarker for predicting the immunotherapy benefits in SKCM. (A) Level of HLA-related genes, (B) immune checkpoints, (C) TMB score, (D) PD1 and CTLA-4 immunophenoscore, (E) TIDE score, (F) immunological escape score and (G) immune surveillance score in patients with SKCM in different risk score categories. (H) Risk score, (I) survival rates and (J) immunotherapy response rate in patients with SKCM with different risk score in the IMvigor210 cohort. (K) Risk score, (L) survival rates and (M) immunotherapy response rate in patients with SKCM with different risk scores in the GSE78220 cohort. (N) Risk score, (O) survival rates and (P) immunotherapy response rate in patients with SKCM with different risk scores in the GSE91061 cohort *P<0.05, **P<0.01 and ***P<0.001. SKCM, skin cutaneous melanoma; HLA, human leukocyte antigen; TMB, tumor mutation burden; PD1, programmed cell death protein-1; CTLA4, cytotoxic T-lymphocyte associated protein 4; TIDE, tumor immune dysfunction and exclusion; GSE, gene expression data series; CR, complete response; PR, partial response; SD, stable disease; PD, progressive disease.

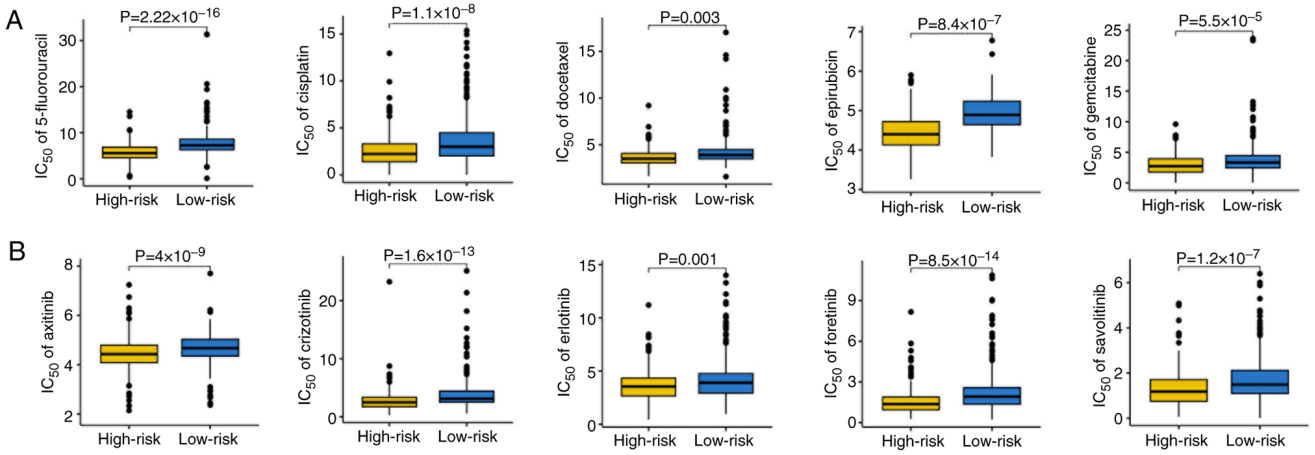

Figure 5. IC_{50} value of drugs in different risk score groups. Patients with SKCM with low-risk score had higher IC_{50} values for drugs correlated with (A) chemotherapy and (B) targeted therapy. SKCM, skin cutaneous melanoma.

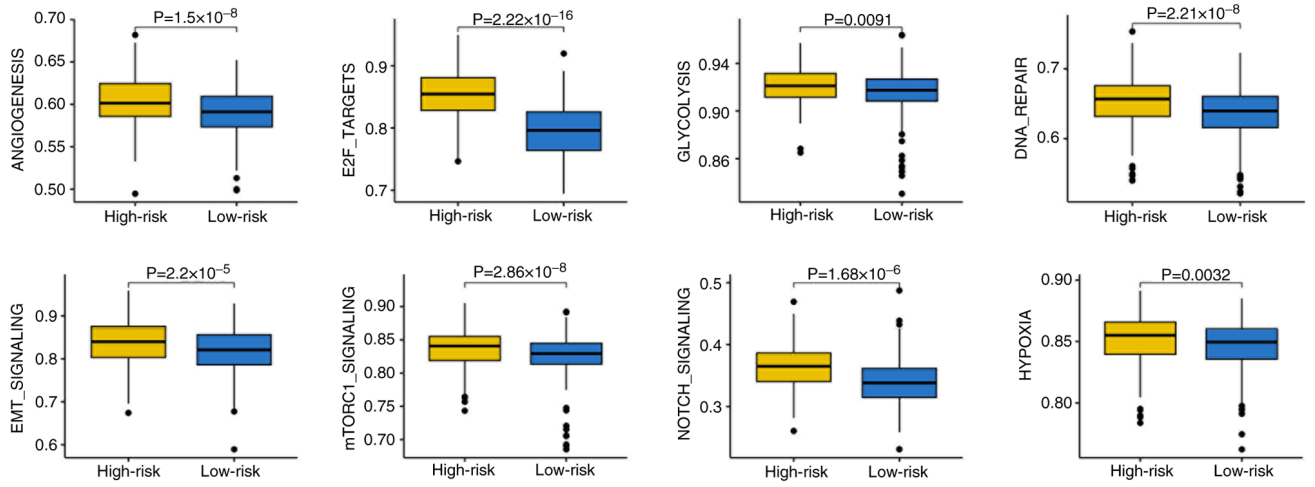

Figure 6. Correlation between cancer-related hallmarks and risk score in SKCM. The gene sets scoring for cancer hallmarks were lower in patients with SKCM with low-risk scores. SKCM, skin cutaneous melanoma; E2F, early region 2 binding factor; EMT, epithelial-mesenchymal transition.

patients (Fig. 4H-P), confirming the ability of the signature to stratify immunotherapy benefit.

Predictive value for chemotherapy and targeted therapy sensitivity. The present study next explored the association between the risk score and drug sensitivity. Patients with low-risk scores demonstrated significantly higher IC_{50} values for commonly used chemotherapy agents, including 5-fluorouracil, cisplatin, docetaxel, epirubicin and gemcitabine (Fig. 5A), and for several targeted therapies such as axitinib, crizotinib, erlotinib, foretinib and savolitinib (Fig. 5B). These findings suggested that high-risk patients with SKCM may be more sensitive to cytotoxic and targeted drugs, while low-risk patients may derive greater benefit from immunotherapy.

Enrichment of cancer hallmarks in high-risk patients with SKCM. To elucidate the biological pathways associated with different risk groups, the present study performed gene set enrichment analysis. High-risk patients exhibited increased enrichment scores for cancer-related hallmarks, including 'angiogenesis', 'E2F targets', 'glycolysis', 'DNA repair', 'EMT signaling', 'mTORC1 signaling', 'Notch signaling' and 'hypoxia' (Fig. 6). These pathways are well-known to contribute to tumor progression, immune evasion and resistance to therapy, potentially explaining the poor prognosis and lower immunotherapy benefit in high-risk patients.

Validation of SFN as a functional driver gene in SKCM. Among the 13 genes comprising the risk signature, SFN had the highest positive coefficient and was consistently upregulated in SKCM tissues. Immunohistochemistry confirmed elevated SFN protein expression in SKCM compared with that in normal skin (Fig. 7A). RT-qPCR also demonstrated higher SFN expression in SKCM cell lines compared with that in normal melanocytes of A375 and A2058 melanoma cells (Fig. 7B). The SFN expression of A375 and A2058 melanoma cells were then knocked down (Fig. 7C). Functionally, knockdown of SFN significantly inhibited the proliferation of A375 and A2058 melanoma cells, as shown in the CCK-8 assays (Fig. 7D), supporting its role as an oncogenic driver and validating its inclusion in the risk model.

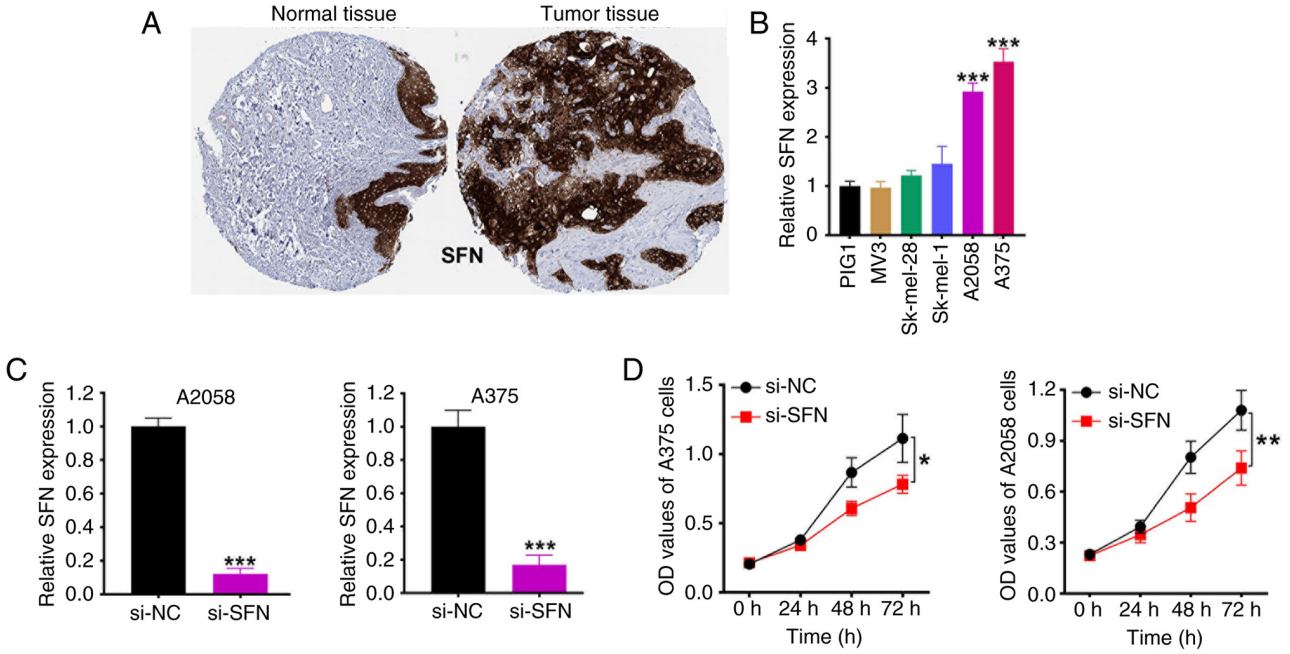

Figure 7. Validating the role of SFN in SKCM. (A) Typical SFN immunohistochemistry in normal and SKCM tissues obtained from the Human Protein Atlas database. (B) The relative SFN expression levels in SKCM and normal cell lines. ***P<0.001 vs. PIG1. (C) Verification of the knockdown effect of SFN. (D) The CCK-8 experiment demonstrated that downregulation of SFN clearly reduced A375 and A2058 cell proliferation. *P<0.05, **P<0.01 and ***P<0.001. SFN, stratifin; SKCM, skin cutaneous melanoma; CCK-8, Cell Counting Kit-8; NC, negative control.

Discussion

In the present study, a robust PCDI was developed and validated using integrated machine learning algorithms to predict prognosis and immunotherapy response in patients with SKCM. By integrating multi-cohort data and systematically evaluating 77 algorithm combinations, a 13-gene risk signature that stratifies patients into distinct prognostic and immunological subtypes with high accuracy and clinical relevance was identified.

The present study results demonstrated that the PCDI effectively distinguishes patients with SKCM with poor outcomes from those with favorable survival, as evidenced by consistent results across TCGA and multiple independent GEO cohorts. The model outperformed conventional clinical features such as age, sex and TNM stage in prognostic prediction, which supports its potential clinical utility (36,37). The integration of the risk score into a nomogram further improved individual-level survival prediction and calibration analyses confirmed its accuracy and reliability (37).

Notably, the present study findings highlighted a strong association between the PCDI and the tumor immune microenvironment. High-risk patients exhibited reduced infiltration of $CD8^+$ T cells, M1 macrophages and antigen-presenting cells, alongside lower stromal and immune scores, indicating a more immunosuppressive tumor contexture (38,39). Conversely, low-risk patients demonstrated a more immunoactive landscape with higher expression of HLA genes, immune checkpoints and immune cell infiltration, which suggests a favorable environment for immunotherapeutic intervention (40).

The relevance of PCDI in predicting immunotherapy response was further confirmed by its correlation with multiple immune-related biomarkers. Low-risk patients exhibited higher TMB, immunophenoscores for PD-1/CTLA-4 and lower TIDE and immune escape scores compared with patients with a high-risk score, features known to associate with enhanced response to immune checkpoint blockade (21,41,42). These findings were validated across three independent immunotherapy-treated melanoma cohorts, where low-risk patients demonstrated significantly improved response rates and OS. These results suggested that PCDI could serve as a predictive biomarker to guide immunotherapy decision-making in SKCM (43,44).

Furthermore, the drug sensitivity analysis in the present study indicated that high-risk patients were more sensitive to multiple chemotherapeutic and targeted agents, including 5-fluorouracil, cisplatin and several receptor tyrosine kinase inhibitors (crizotinib, erlotinib and foretinib). This observation implies a potential trade-off in treatment strategy: While low-risk patients may benefit more from immunotherapy, high-risk patients might demonstrate improved response to conventional or targeted cytotoxic treatment (45). These findings underscore the value of PCDI in guiding personalized therapeutic strategies beyond immunotherapy.

Functional and pathway enrichment analyses revealed that high-risk patients with SKCM were enriched in oncogenic pathways such as glycolysis, E2F signaling, DNA repair, EMT and hypoxia, all of which are known to contribute to tumor progression, resistance to therapy and immune evasion (14-16). These molecular characteristics likely explain the poor prognosis and reduced immune responsiveness observed in the high-risk group.

Among the 13 genes in the PCDI, SFN emerged as a potential oncogenic driver in SKCM. The high expression levels of SFN were validated at both the transcriptomic

and protein levels and functional assays confirmed its role in promoting melanoma cell proliferation. These findings suggested that SFN may not only serve as a biomarker but also represent a potential therapeutic target in high-risk SKCM. A previous study reported that upregulation of SFN was associated with the prognosis in ovarian cancer (46). Furthermore, SFN regulates cervical cancer cell proliferation, apoptosis and metastasis progression through Lin-11, Isl-1 and Mec-3 domain kinase 2/cofilin signaling (47).

Despite the strengths of the present study, including a large sample size, cross-cohort validation and integration of multi-dimensional data, several limitations should be acknowledged. First, the retrospective nature of the datasets may introduce biases that could affect generalizability. Second, although the immunotherapy response predictions were validated in public cohorts, prospective clinical validation is warranted to confirm the utility of PCDI in guiding treatment decisions. Lastly, while SFN was functionally validated, the biological roles of other model genes warrant further investigation.

Further understanding of the molecular mechanisms through which PCDI-related genes contribute to melanoma progression and immune modulation is essential. For instance, SFN, identified as a key oncogenic driver in the present study model, is involved in cell proliferation control. However, its downstream effectors in the context of SKCM remain poorly characterized. Future studies could explore whether SFN modulates tumor progression and immune evasion pathways, such as PD-L1 expression or antigen presentation machinery. While the present study PCDI demonstrated predictive power across public immunotherapy cohorts, validation in prospective, cohorts including treatment-naïve patients with SKCM is imperative. Ideally, this would involve enrolling patients prior to immunotherapy, obtaining baseline biopsies for transcriptomic profiling, calculating PCDI scores and associating them with clinical outcomes such as Response Evaluation Criteria in Solid Tumors response, progression-free survival and OS.

In conclusion, the present study developed a novel machine learning-based PCDI that robustly predicts prognosis and immunotherapy response in SKCM. The index provides valuable insights into tumor biology and immune phenotypes and holds potential as a biomarker for personalized therapy in patients with melanoma. Future studies integrating multi-omics and experimental validation will further refine and extend the clinical utility of the present study model.

Acknowledgements

Not applicable.

Funding

No funding was received.

Availability of data and materials

The data generated in the present study may be requested from the corresponding author.

Authors' contributions

XW prepared the original draft. XW and YZ performed the investigation. YZ conducted the formal analysis and curated the data. SY and HS acquired data, and reviewed and edited the manuscript. WC and SS analyzed and interpreted the data, and were involved in project administration. XW and YZ confirm the authenticity of all the raw data. All authors read and approved the final manuscript.

Ethics approval and consent to participate

Not applicable.

Patient consent for publication

Not applicable.

Competing interests

The authors declare that they have no competing interests.

References

1. Long GV, Swetter SM, Menzies AM, Gershenwald JE and Scolyer RA: Cutaneous melanoma. Lancet 402: 485-502, 2023.
2. Arnold M, Singh D, Laversanne M, Vignat J, Vaccarella S, Meheus F, Cust AE, de Vries E, Whiteman DC and Bray F: Global burden of cutaneous melanoma in 2020 and projections to 2040. JAMA Dermatol 158: 495-503, 2022.
3. Lopes F, Sleiman MG, Sebastian K, Bogucka R, Jacobs EA and Adamson AS: UV exposure and the risk of cutaneous melanoma in skin of color: A systematic review. JAMA Dermatol 157: 213-219, 2021.
4. Leonardi GC, Falzone L, Salemi R, Zanghì A, Spandidos DA, Mccubrey JA, Candido S and Libra M: Cutaneous melanoma: From pathogenesis to therapy (Review). Int J Oncol 52: 1071-1080, 2018.
5. Newton K, Strasser A, Kayagaki N and Dixit VM: Cell death. Cell 187: 235-256, 2024.
6. Liu J, Hong M, Li Y, Chen D, Wu Y and Hu Y: Programmed cell death tunes tumor immunity. Front Immunol 13: 847345, 2022.
7. Liang T, Gu L, Kang X, Li J, Song Y, Wang Y and Ma W: Programmed cell death disrupts inflammatory tumor microenvironment (TME) and promotes glioblastoma evolution. Cell Commun Signal 22: 333, 2024.
8. Liu Y, Shou Y, Zhu R, Qiu Z, Zhang Q and Xu J: Construction and validation of a ferroptosis-related prognostic signature for melanoma based on single-cell RNA sequencing. Front Cell Dev Biol 10: 818457, 2022.
9. Nedaeinia R, Dianat-Moghadam H, Movahednasab M, Khosroabadi Z, Keshavarz M, Amoozgar Z and Salehi R: Therapeutic and prognostic values of ferroptosis signature in glioblastoma. Int Immunopharmacol 155: 114597, 2025.
10. Wang S, Wang R, Hu D, Zhang C, Cao P and Huang J: Machine learning reveals diverse cell death patterns in lung adenocarcinoma prognosis and therapy. NPJ Precis Oncol 8: 49, 2024.
11. Zhang L, Cui Y, Zhou G, Zhang Z and Zhang P: Leveraging mitochondrial-programmed cell death dynamics to enhance prognostic accuracy and immunotherapy efficacy in lung adenocarcinoma. J Immunother Cancer 12: e010008, 2024.
12. Cai X, Lin J, Liu L, Zheng J, Liu Q, Ji L and Sun Y: A novel TCGA-validated programmed cell-death-related signature of ovarian cancer. BMC Cancer 24: 515, 2024.
13. Wang Y and Zhang Q: Leveraging programmed cell death signature to predict clinical outcome and immunotherapy benefits in postoperative bladder cancer. Sci Rep 14: 22976, 2024.
14. Gu X, Pan J, Li Y and Feng L: A programmed cell death-related gene signature to predict prognosis and therapeutic responses in liver hepatocellular carcinoma. Discov Oncol 15: 71, 2024.
15. Nayarisseri A, Khandelwal R, Tanwar P, Madhavi M, Sharma D, Thakur G, Speck-Planche A and Singh SK: Artificial intelligence, big data and machine learning approaches in precision medicine & drug discovery. Curr Drug Targets 22: 631-655, 2021.

16. Ngiam KY and Khor IW: Big data and machine learning algorithms for health-care delivery. Lancet Oncol 20: e262-e273, 2019.
17. Jayawardana K, Schramm SJ, Haydu L, Thompson JF, Scolyer RA, Mann GJ, Müller S and Yang JY: Determination of prognosis in metastatic melanoma through integration of clinico-pathologic, mutation, mRNA, microRNA, and protein information. Int J Cancer 136: 863-874, 2015.
18. Budden T, Davey RJ, Vilain RE, Ashton KA, Braye SG, Beveridge NJ and Bowden NA: Repair of UVB-induced DNA damage is reduced in melanoma due to low XPC and global genome repair. Oncotarget 7: 60940-60953, 2016.
19. Cabrita R, Lauss M, Sanna A, Donia M, Skaarup Larsen M, Mitra S, Johansson I, Phung B, Harbst K, Vallon-Christersson J, *et al*: Tertiary lymphoid structures improve immunotherapy and survival in melanoma. Nature 577: 561-565, 2020.
20. Riaz N, Havel JJ, Makarov V, Desrichard A, Urba WJ, Sims JS, Hodi FS, Martín-Algarra S, Mandal R, Sharfman WH, *et al*: Tumor and microenvironment evolution during immunotherapy with nivolumab. Cell 171: 934-949.e16, 2017.
21. Hugo W, Zaretsky JM, Sun L, Song C, Moreno BH, Hu-Lieskovan S, Berent-Maoz B, Pang J, Chmielowski B, Cherry G, *et al*: Genomic and transcriptomic features of response to Anti-PD-1 therapy in metastatic melanoma. Cell 165: 35-44, 2016.
22. Rosenberg JE, Galsky MD, Powles T, Petrylak DP, Bellmunt J, Loriot Y, Necchi A, Hoffman-Censits J, Perez-Gracia JL, van der Heijden MS, *et al*: Atezolizumab monotherapy for metastatic urothelial carcinoma: Final analysis from the phase II IMvigor210 trial. ESMO Open 9: 103972, 2024.
23. Ritchie ME, Phipson B, Wu D, Hu Y, Law CW, Shi W and Smyth GK: Limma powers differential expression analyses for RNA-sequencing and microarray studies. Nucleic Acids Res 43: e47, 2015.
24. Liu Z, Liu L, Weng S, Guo C, Dang Q, Xu H, Wang L, Lu T, Zhang Y, Sun Z and Han X: Machine learning-based integration develops an immune-derived lncRNA signature for improving outcomes in colorectal cancer. Nat Commun 13: 816, 2022.
25. Sturm G, Finotello F and List M: Immunedeconv: An R package for unified access to computational methods for estimating immune cell fractions from bulk RNA-sequencing data. Methods Mol Biol 2120: 223-232, 2020.
26. Yoshihara K, Shahmoradgoli M, Martínez E, Vegesna R, Kim H, Torres-Garcia W, Treviño V, Shen H, Laird PW, Levine DA, *et al*: Inferring tumour purity and stromal and immune cell admixture from expression data. Nat Commun 4: 2612, 2013.
27. Palmeri M, Mehnert J, Silk AW, Jabbour SK, Ganesan S, Popli P, Riedlinger G, Stephenson R, de Meritens AB, Leiser A, *et al*: Real-world application of tumor mutational burden-high (TMB-high) and microsatellite instability (MSI) confirms their utility as immunotherapy biomarkers. ESMO Open 7: 100336, 2022.
28. Fu J, Li K, Zhang W, Wan C, Zhang J, Jiang P and Liu XS: Large-scale public data reuse to model immunotherapy response and resistance. Genome Med 12: 21, 2020.
29. Charoentong P, Finotello F, Angelova M, Mayer C, Efremova M, Rieder D, Hackl H and Trajanoski Z: Pan-cancer immunogenomic analyses reveal genotype-immunophenotype relationships and predictors of response to checkpoint blockade. Cell Rep 18: 248-262, 2017.
30. Sun Y, Wu L, Zhong Y, Zhou K, Hou Y, Wang Z, Zhang Z, Xie J, Wang C, Chen D, *et al*: Single-cell landscape of the ecosystem in early-relapse hepatocellular carcinoma. Cell 184: 404-421.e16, 2021.
31. Maeser D, Gruener RF and Huang RS: oncoPredict: An R package for predicting in vivo or cancer patient drug response and biomarkers from cell line screening data. Brief Bioinform 22: bbab260, 2021.
32. Livak KJ and Schmittgen TD: Analysis of relative gene expression data using real-time quantitative PCR and the 2(-Delta Delta C(T)) Method. Methods 25: 402-408, 2001.
33. Balch CM, Gershenwald JE, Soong SJ, Thompson JF, Atkins MB, Byrd DR, Buzaid AC, Cochran AJ, Coit DG, Ding S, *et al*: Final version of 2009 AJCC melanoma staging and classification. J Clin Oncol 27: 6199-6206, 2009.
34. Lin A and Yan WH: HLA-G/ILTs targeted solid cancer immunotherapy: Opportunities and challenges. Front Immunol 12: 698677, 2021.
35. Lin A, Zhang J and Luo P: Crosstalk between the MSI status and tumor microenvironment in colorectal cancer. Front Immunol 11: 2039, 2020.
36. Siegel RL, Miller KD, Wagle NS and Jemal A: Cancer statistics, 2023. CA Cancer J Clin 73: 17-48, 2023.
37. Gershenwald JE, Scolyer RA, Hess KR, Sondak VK, Long GV, Ross MI, Lazar AJ, Faries MB, Kirkwood JM, McArthur GA, *et al*: Melanoma staging: Evidence-based changes in the American Joint Committee on Cancer eighth edition cancer staging manual. CA Cancer J Clin 67: 472-492, 2017.
38. Wang J, Yang F, Sun Q, Zeng Z, Liu M, Yu W, Zhang P, Yu J, Yang L, Zhang X, *et al*: The prognostic landscape of genes and infiltrating immune cells in cytokine induced killer cell treated-lung squamous cell carcinoma and adenocarcinoma. Cancer Biol Med 18: 1134-1147, 2021.
39. Tien FM, Lu HH, Lin SY and Tsai HC: Epigenetic remodeling of the immune landscape in cancer: Therapeutic hurdles and opportunities. J Biomed Sci 30: 3, 2023.
40. Rooney MS, Shukla SA, Wu CJ, Getz G and Hacohen N: Molecular and genetic properties of tumors associated with local immune cytolytic activity. Cell 160: 48-61, 2015.
41. Sun R, Limkin EJ, Vakalopoulou M, Champiat S, Han SR, Verlingue L, Brandao D, Lancia A, Ammari S, Hollebecque A, *et al*: A radiomics approach to assess tumour-infiltrating CD8 cells and response to anti-PD-1 or anti-PD-L1 immunotherapy: an imaging biomarker, retrospective multicohort study. Lancet Oncol 19: 1180-1191, 2018.
42. Jiang P, Gu S, Pan D, Fu J, Sahu A, Hu X, Li Z, Traugh N, Bu X, Li B, *et al*: Signatures of T cell dysfunction and exclusion predict cancer immunotherapy response. Nat Med 24: 1550-1558, 2018.
43. Liu D, Schilling B, Liu D, Sucker A, Livingstone E, Jerby-Arnon L, Zimmer L, Gutzmer R, Satzger I, Loquai C, *et al*: Integrative molecular and clinical modeling of clinical outcomes to PD1 blockade in patients with metastatic melanoma. Nat Med 25: 1916-1927, 2019.
44. Gide TN, Quek C, Menzies AM, Tasker AT, Shang P, Holst J, Madore J, Lim SY, Velickovic R, Wongchenko M, *et al*: Distinct immune cell populations define response to anti-PD-1 monotherapy and anti-PD-1/Anti-CTLA-4 combined therapy. Cancer Cell 35: 238-255.e6, 2019.
45. Yang W, Soares J, Greninger P, Edelman EJ, Lightfoot H, Forbes S, Bindal N, Beare D, Smith JA, Thompson IR, *et al*: Genomics of drug sensitivity in cancer (GDSC): A resource for therapeutic biomarker discovery in cancer cells. Nucleic Acids Res 41(Database Issue): D955-D961, 2013.
46. Hu Y, Zeng Q, Li C and Xie Y: Expression profile and prognostic value of SFN in human ovarian cancer. Biosci Rep 39: BSR20190100, 2019.
47. Du N, Li D, Zhao W and Liu Y: Stratifin (SFN) regulates cervical cancer cell proliferation, apoptosis, and cytoskeletal remodeling and metastasis progression through LIMK2/cofilin signaling. Mol Biotechnol 66: 3369-3381, 2024.